Digest Journal of Nanomaterials and Biostructures Vol. 7, No. 2, April - June 2012, p. 563 - 576

COMBINATORIAL PULSED LASER DEPOSITION OF AG-CONTAINING CALCIUM PHOSPHATE COATINGS

G. SOCOL[a*], M. SOCOL[b], L. SIMA[c], S. PETRESCU[c], M. ENCULESCU[b], F. SIMA[a], M. MIROIU[a], G. POPESCU-PELIN[a], N. STEFAN[a], R. CRISTESCU[a], C.N. MIHAILESCU[a], A. STANCULESCU[b], C. SUTAN[d], I.N. MIHAILESCU[a]
[a]*National Institute for Lasers, Plasma and Radiation Physics, Magurele, Ilfov, Romania*
[b]*National Institute of Materials Physics, Magurele, Ilfov, Romania*
[c]*Institute of Biochemistry, Splaiul Independentei 296, Bucharest, Romania*
[d]*University of Pitesti, Research Centre for Advanced Materials, Targul din Vale Street, No 1, 110040, Pitesti, Arges, Romania*

Embedding silver (Ag) into CaPs one could expect the enhancement of the antimicrobial performances of coatings for load bearing implants. The aim of this research was to evaluate whether the cellular morphology is influenced by the variation of Ag content, as well as by the solubility and morphological features of Ag-containing CaP coatings obtained by combinatorial pulsed laser deposition technique. In this view, we developed compositional libraries of either Ag and hydroxyapatite (HA) or Ag and β-tricalcium phosphate (β–TCP). The Ag content along the length of the combinatorial CaP coatings increased up to a maximum of ~1 at.%. SEM and AFM images evidenced the abundant presence of particulates typical for CaP coatings deposited by PLD. AFM histograms showed that the samples were rough with RMS values within 61-209 nm range. Ag content values up to 0.6 at. % into HA coatings were found nontoxic for mesenchymal stem cell (MSC) growth.

(Received April 6, 2012; Accepted April 12, 2012)

Keywords: Silver doping, Calcium Phosphates, Combinatorial PLD, **M**esenchymal stem cells

1. Introduction

Calcium phosphates (CaPs) are the most widely used bone substitutes in tissue engineering due to their similarity with the inorganic bone composition and excellent biocompatibility. Because of their poor mechanical properties CaPs are frequently deposited as coatings on metallic implants [1] combining the benefits of bioactive thin coatings and the mechanical strength of the substrate [2-4] CaPs are characterized by different dissolution rates given by the Ca/P ratios. Hydroxyapatite (HA) is the main inorganic compound in bone as well as the most stable and the least soluble biocompatible calcium phosphate MCP>TTCP>α-TCP>DCPD>DCP>OCP>β-TCP>CDHA> HA (with Monocalcium phosphate = MCP, Tetracalcium phosphate = TTCP, α -Tricalcium phosphate = α-TCP, Dicalcium phosphate dihydrate = DCPD, Octacalcium phosphate = OCP, β-Tricalcium phosphate = β-TCP, Calcium-deficient hydroxyapatite = CDHA, Hydroxyapatite = HA) [2, 5, 6]. β-tricalcium phosphate (β-TCP) is a bio-resorbable material quite appropriate for bone augmentation in clinical situations [7-10]. Considered as a bone biodegradable substitute, once introduced within the body β-TCP is gradually replaced by newly mineralizing bone avoiding fibrous tissue encapsulation [11, 12]. The integration of implants within the surrounding bone strongly depends on bone - implant interface

*Corresponding author: gabriel.socol@inflpr.ro

characteristics. Thus, a proper interaction results in a long term stabilization of implant. However, bone healing process is prone to infections if bacteria colonies appear at the interface. This might further lead to implant failure. In order to reduce the incidence of implant-associated infections, different surface improvement strategies have been proposed. Among these strategies, the antimicrobial drug delivery systems play a significant role [13-15]. On the other hand, metals (such as Ag, Cu or Zn) were widely used in medicine as antimicrobial agents. Silver and silver-based compounds are known as medical agents with excellent antibacterial action [16-18]. These properties are typical for heavy metals but, unlike them, silver is characterized by reduced toxicity to human cells [19-21]. Therefore, the Ag-containing biomaterials are considered potential candidates for wound repair applications [21-23]. It was confirmed that both ionic and metallic forms of silver shows relatively low toxicity to human cells [21, 23]. Silver has been incorporated into several biomaterials such as polyurethane [21], HA [19, 25] and bioactive glasses [26-28]. Most of results based on Ag-containing CaP coatings report antibacterial activity against a wide variety of bacteria but just a few studies are devoted to the cellular response. Pulsed Laser Deposition (PLD) is a versatile technique able to produce coatings with the same stoichiometry of the initial raw material [4]. PLD was frequently applied to obtain calcium phosphate coatings with good physico-chemical and biological properties [29-32]. An extension of PLD, Combinatorial Pulsed Laser Deposition (CPLD), was proposed for the fabrication of thin films with gradual modification of elemental composition along the substrate surface by simultaneous ablation of two or more targets [4, 33]. We propose the extension of CPLD to biomaterials and, in particular, to calcium phosphate coatings in order to produce complex gradient libraries of either Ag and HA, Ag:HA or Ag and β –TCP, Ag:β –TCP. The aim was to evaluate the toxicity to human cells of HA and β-TCP thin films containing different concentrations of Ag obtained by CPLD technique.

2. Material and methods

Combinatorial pulsed laser deposition

CPLD experiments were conducted into a UHV deposition chamber using a typical combinatorial geometry illustrated in Figure 1 [33]. Two batches of combinatorial Ag:CaP (Ag+HA or Ag+ β-TCP) samples were deposited on glass slides of 76x6.5 mm^2 using two targets, i. e. metallic Ag (99.95% purity) and either HA or β-TCP (Table I). HA and β-TCP targets were manufactured by pressing the powders at 5 MPa and sintering in air for 6 hours at 400 ^oC and 1100 ^oC, respectively. The coatings were deposited by simultaneous ablation of two targets (Ag and Ha or β-TCP) using a KrF* (λ= 248 nm, τ_{FWHM} = 25 ns) laser source (model COMPexPro 205, Lambda Physics-Coherent). The depositions were carried out at room temperature in a continuous flow of O_2 at 10 Pa dynamic pressure. Laser fluence was set at 1 Jcm^{-2} and frequency repetition rate was 10 Hz. All coatings were grown at a target-substrate separation distance of 5 cm by applying 5,000 subsequent laser pulses on each target. Prior to introduction inside the deposition chamber, the substrates were successively cleaned into an ultrasonic bath with acetone, ethanol and deionized water for 15 min and then dried in a jet of high purity nitrogen. In order to obtain comparable results, the positions of the targets and substrates in respect to the laser beam focus points were identical in all experiments. In our setup the separation distance between the irradiation spots on targets is D =50 mm, equal to the distance between A and B points on substrate (Fig. 1). We therefore consider "A" and "B" as the points of coordinates 0 and 50 mm on substrate. We deposited films with a well-defined gradient of composition along the length of the glass slide.

Table I. Deposition conditions of combinatorial Ag-doped HA and β-TCP coatings

Combinatorial PLD sample	Target 1	Target 2	Laser Fluence Target 1 (J/cm^2)	Laser Fluence Target 2 (J/cm^2)	No. of pulses
Ag-HA	Ag		1		5000
		HA		1	5000
Ag-β-TCP	Ag		1		5000
		β -TCP		1	5000

Table II. RMS values of combinatorial Ag-containing HA and β-TCP coatings estimated from different areas between d= 0 mm and d= 50 mm

Position d (mm)	0 (“A”)	10	20	30	40	50 (“B”)
Sample	Ag-HA	Ag-HA	Ag-HA	Ag-HA	Ag-HA	Ag-HA
RMS (nm)	61	133	124	118	155	209
Sample	Ag-β-TCP	Ag-β-TCP	Ag-β-TCP	Ag-β-TCP	Ag-β-TCP	Ag-β-TCP
RMS (nm)	55	66	92	87	133	169

Morphological studies

The morphological features of the films were examined by Atomic Force Microscopy (AFM) in tapping mode with a Nanonics MV 4000 Microscope. AFM images were recorded on 20x20 μm^2 areas. Scanning Electron Microscopy (SEM) investigation was performed with an EVO 50XVP Carl Zeiss microscope with LaB_6 filament and a maximum accelerating voltage of 10kV. Because the samples were electrically nonconductive the coatings were capped with thin Au films. An energy dispersive X-ray spectroscope (EDX) model Quantax Bruker 200 with Peltier cooled X-ray detector was used to determine the Ag atomic content (at.%) profile and 2D mapping of elemental composition.

Biocompatibility assays

All tested materials were sterilized by incubation in a solution of 1% penicillin / streptomycin for 2 h, followed by two washes in phosphate buffer saline (PBS) prior to cell culture. Mesenchymal stem cells (MSCs) were cultured in Dulbecco’s Modified Eagle’s Media (DMEM) supplemented with 10% FCS (Biochrom AG), 1% Glutamax, 50 U / mL penicillin, and 50 mg / mL streptomycin (Gibco). They were split 1:2 every 10 days and cultured in a 5% CO 2 humid atmosphere at 37 °C. For the biocompatibility experiments, 110000 cells were seeded per 1 mL warm media per slide in 10 cm Petri dishes (TPP). Samples were left stand for 30 minutes to allow cells to attach to the biomaterial surface and then warm media was added to cover them (5 mL/dish). MSCs were incubated for the indicated time periods. Cells were fixed at 3h, 6h and 24h after seeding using 4% p-formaldehyde (PFA) solution in PBS for 10 min at room temperature (RT). Plates were washed with PBS and stored at 4°C before use. MSCs were stained for 3 hours at RT with 0.4% crystal violet solution in 20% ethanol and kept in dH2O until analysis. Cells distribution and spreading along the combinatorial samples were investigated using a Nikon Eclipse E600W epifluorescence microscope in the bright field setting. Pictures were taken using a Nikon digital light DS-SM camera and NIS-Elements BR Software. Statistical estimations of MSC perimeters and areas were evaluated using ImageJ Software.

3. Results and discussion

Morphological results

Sample properties were analyzed along the AB direction (Fig 1). AFM and SEM analyses revealed differences in surface topography along this direction, with distinctive features specific to each combinatorial Ag:CaP system. The morphology is generally characterized by irregular and granular structures consisting of particulates with dimensions in the sub- micrometer and micrometer range (Figs. 2-3) and grains with tens or hundreds of nanometers in size (Figs. 4-5). The analysis of AFM histograms revealed that the combinatorial Ag:HA coatings are rather rough, with RMS values varying within the 61-209 nm range (Table I). The lowest and the highest values correspond to the boundaries, i.e. “A” and “B” points (Fig. 3a and Fig. 3f). In-between these positions the RMS values varied within a relatively narrow range (118-155 nm) (Figs. 3b-e). In the case of combinatorial Ag-containing β-TCP coatings we observed a gradual increase of RMS values between “A” and “B” (Figs. 5a-f) from 55 nm to 169 nm (Table I). However, particulates' density and RMS roughness values measured for Ag-β-TCP coatings were in this case slightly lower (Figs. 4-5). SEM and AFM images show similar nanometer and micrometer features but with different topographies characteristic for each CaP system deposited by PLD [29-32]. In general, one observes an increase of particulates' density between “A” and “B”, which is more

pronounced in the case of combinatorial Ag-HA samples. An Ag coating obtained by PLD under the conditions applied in these CPLD experiments had 8 nm RMS roughness. Thus, we concluded that the nano- and micro-roughness and the topography of combinatorial samples are dominated by the morphology of CaP coatings obtained by PLD [29-32]. Micrometer spherical-particulates characteristic to metallic PLD coatings are also visible on the surface or partially embedded into the coatings (Figs. 2a-b and Figs. 3a-c). Nevertheless, Ag particulates' density was significantly lower than those of CaP. Moreover, in the AFM images (Figs. 5a-c) of Ag-β-TCP samples we noticed the presence of holes with diameters in sub-micrometer range. These holes could be formed by the penetration of small Ag particulates with high kinetic energy into the softer β-TCP coatings. CaP particulates visible on the coating surface are flat with irregular shapes. The distribution of particulates' density is a result of plasma plume expansion geometry characteristic to laser ablation, where most of the evaporated species are confined inside a limited and well defined volume [4]. It is worth mentioning that such topologies were proved beneficial for adhesion and proliferation of osteoblast cells [30, 32, 34].

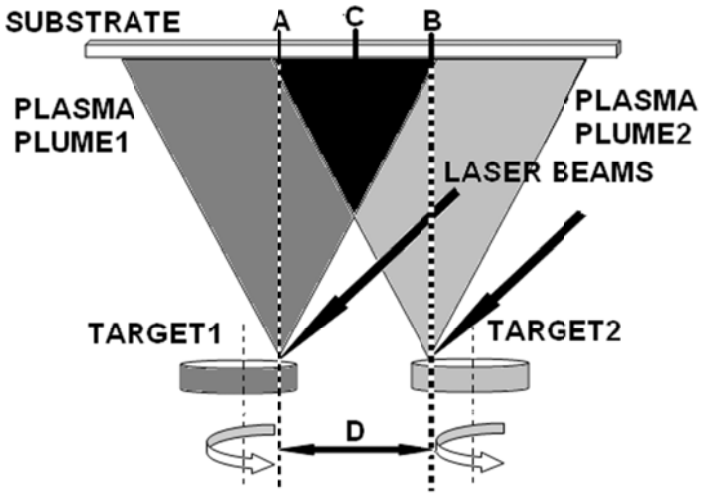

Fig.1 Combinatorial PLD scheme.

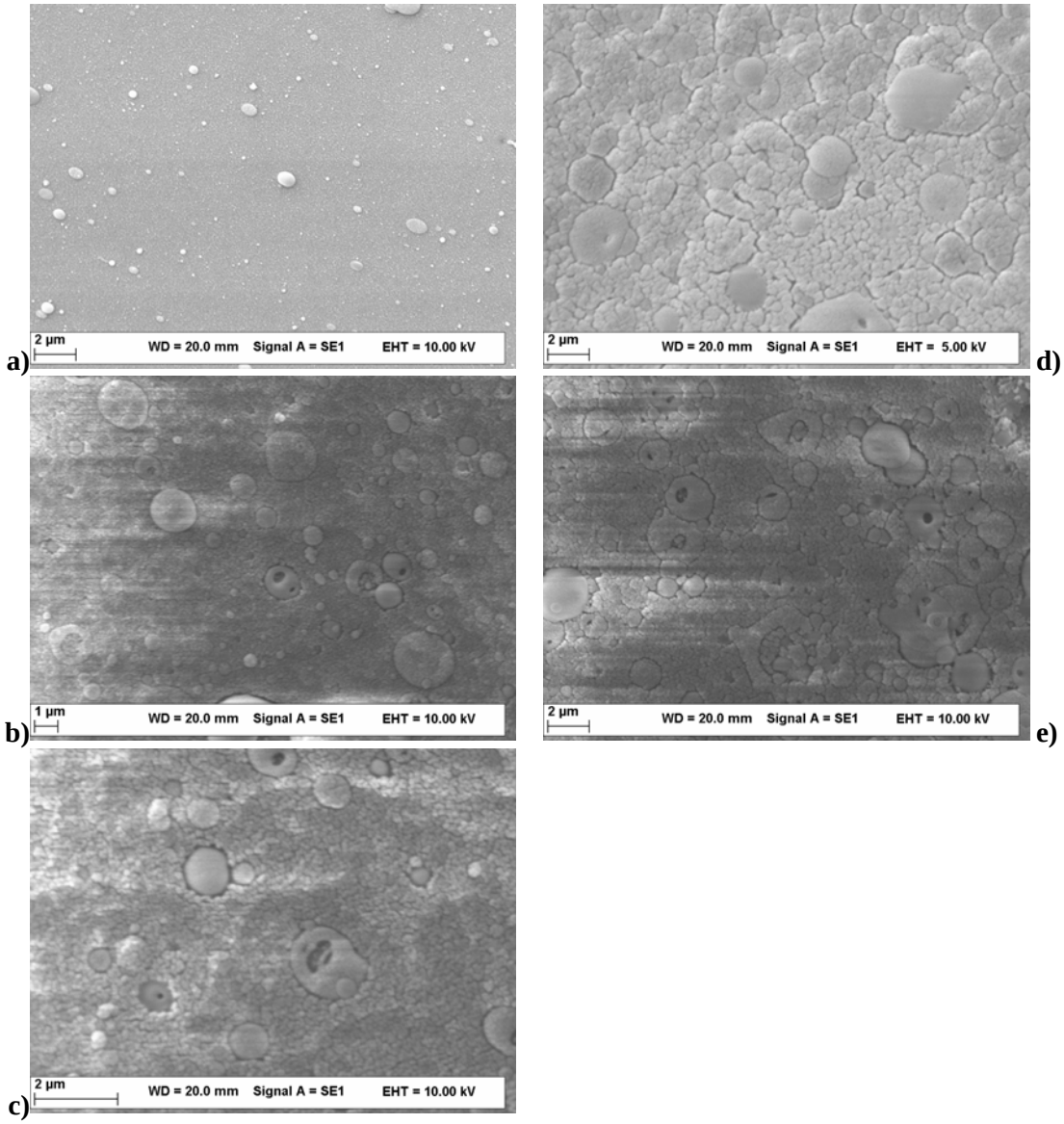

Fig. 2 Typical SEM micrographs of Ag:HA film surface between A and B points at : 0 mm a), 13 mm b), 25 mm c), 38 mm d) and 50 mm e), respectively.

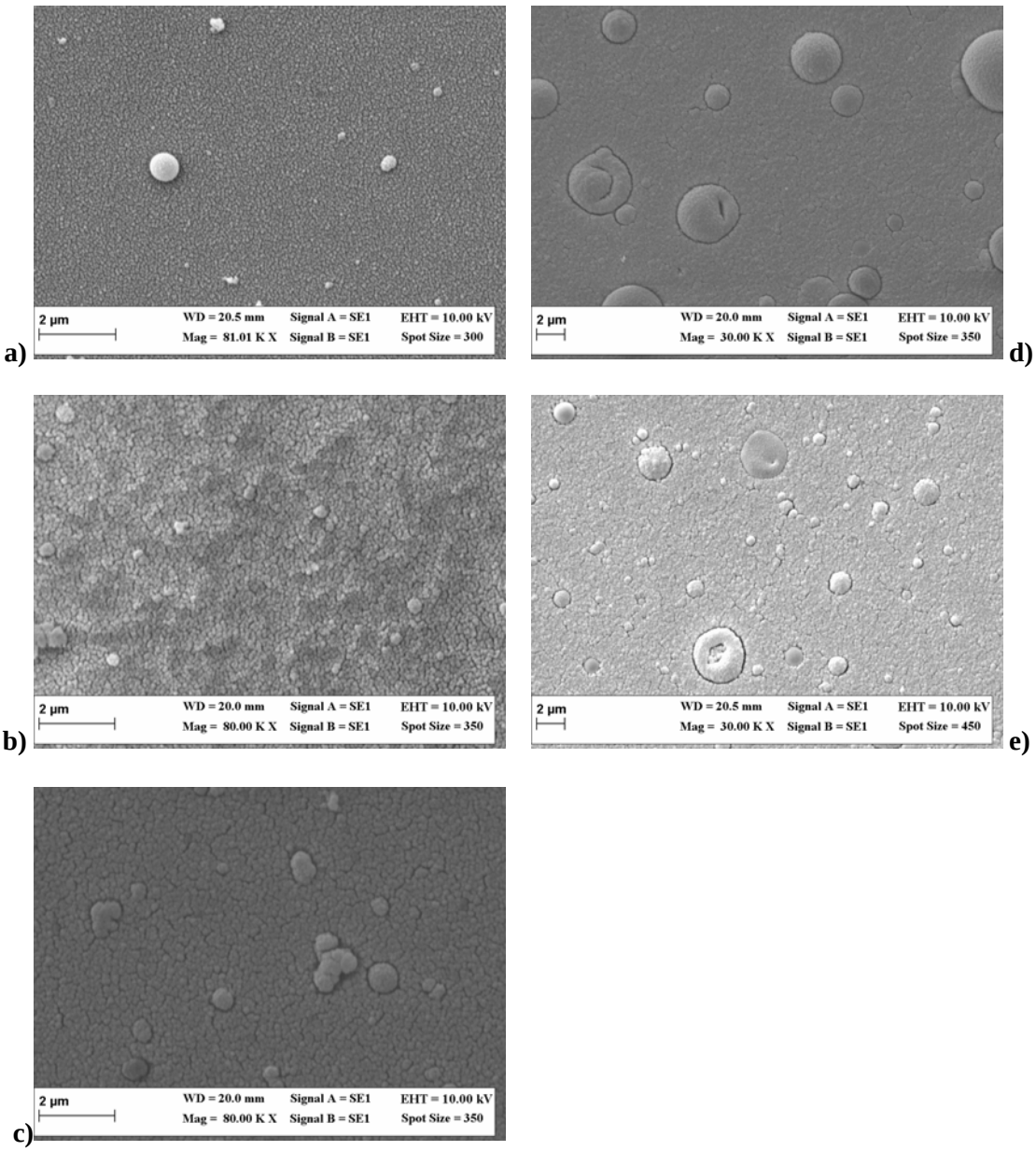

Fig. 3 Typical SEM images of Ag-β-TCP film surface between A and B points at: 0 mm a), 13 mm b), 25 mm c), 38 mm d) and 50 mm e), respectively.

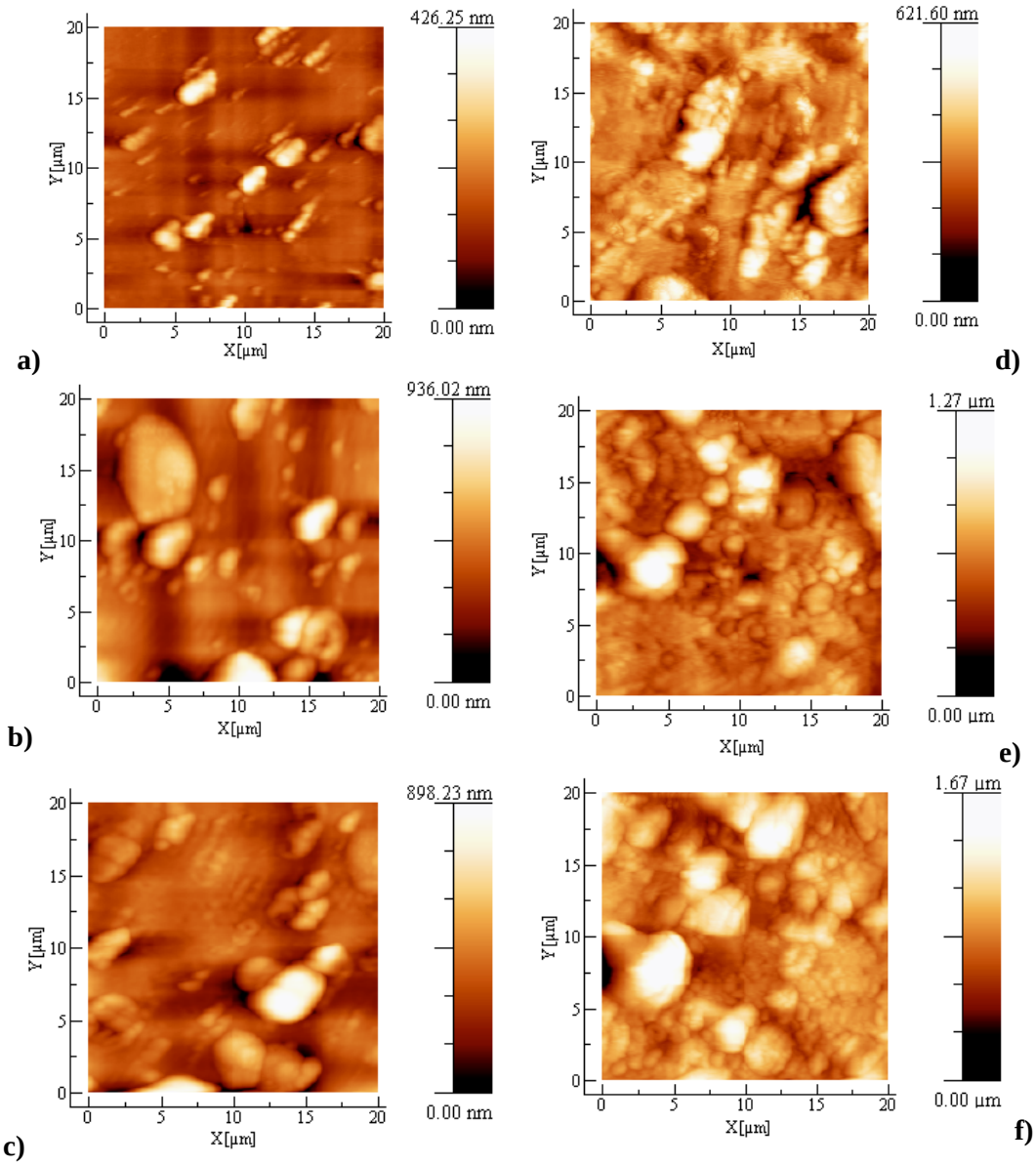

Fig. 4 Typical AFM images of Ag-HA film surface between A and B points: a) 0 mm, b) 10 mm, c) 20 mm, d) 30 mm, e) 40 mm and f) 50 mm, respectively.

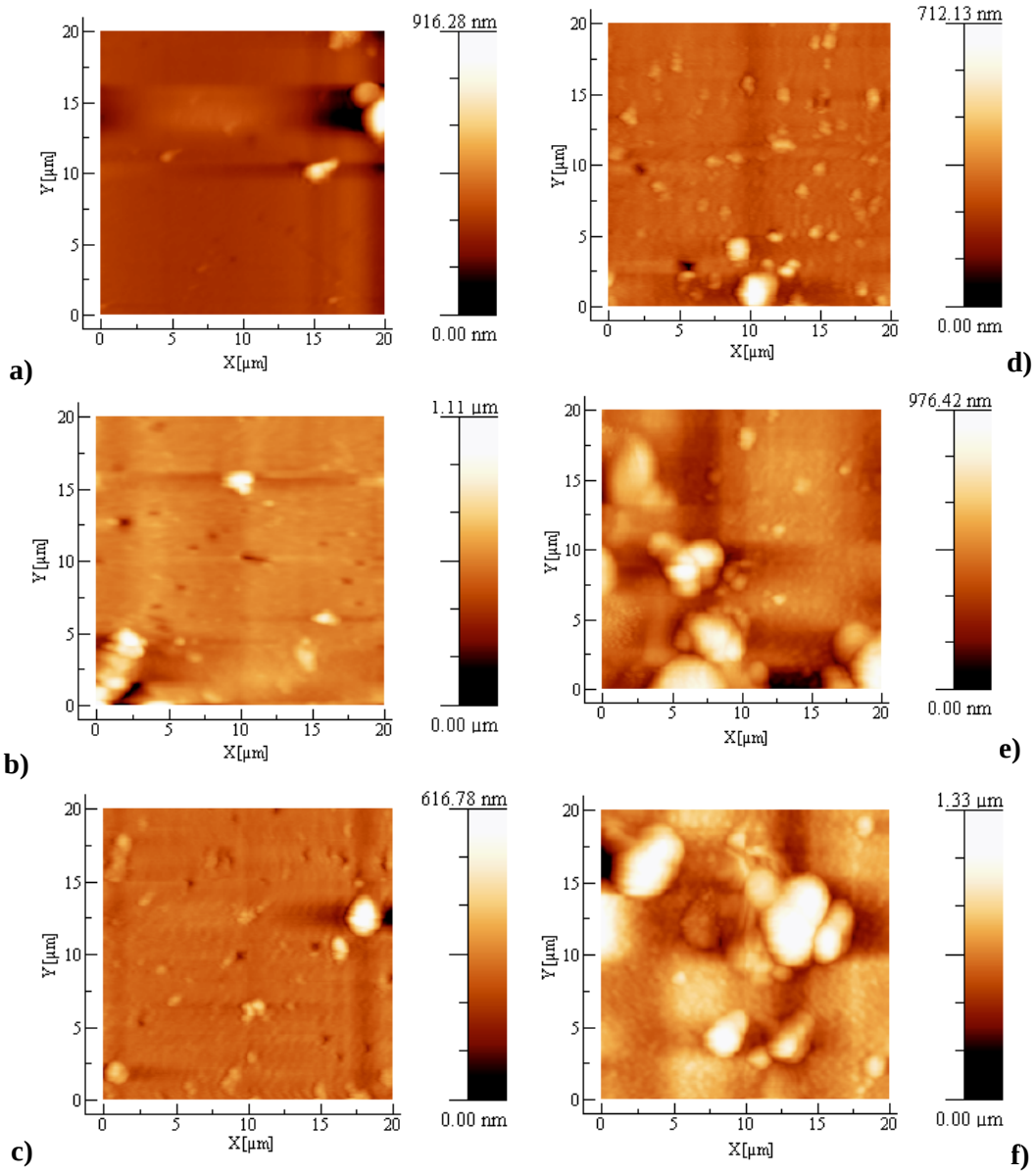

Fig. 5 Typical AFM images of Ag- β-TCP film surface between A and B points: a) 0 mm, b) 10 mm, c) 20 mm, d) 30 mm, e) 40 mm and f) 50 mm, respectively.

Compositional results

In order to establish the Ag content profiles we performed energy dispersive spectrometry (EDS) measurements along the "AB" line (Figs. 6a and b). As expected, for both combinatorial samples, Ag content was the highest in position "A" (0 mm) with values of 0.88 at. % and 0.94 at. % for Ag-HA and Ag- β-TCP, respectively. Ag content linearly decreases from "A" to B" down to 0.14 at. % (Ag-HA) and 0.16 at. % (Ag- β-TCP). The optical spectrum recorded in the case of simple Ag deposition indicated a Surface Plasmon Resonance (SPR) behavior evidenced by the presence of the absorption peak centered around 440 nm (see Fig. 7), characteristic to Ag clusters or very thin films (few tens of nm) [35-37]. The typical thickness profile of PLD films is generally described by a nonlinear function [33, 38]. Consequently, Ag elemental composition profiles should follow the same dependence with the thickness variation. However, the presence of large Ag particulates of sub-micronic or micronic size strongly influnces this profile which becomes quite linear. The effect is visible in Figs 6 a, b because, most probably, the fraction of Ag in particulates is larger or comparable to that in film.

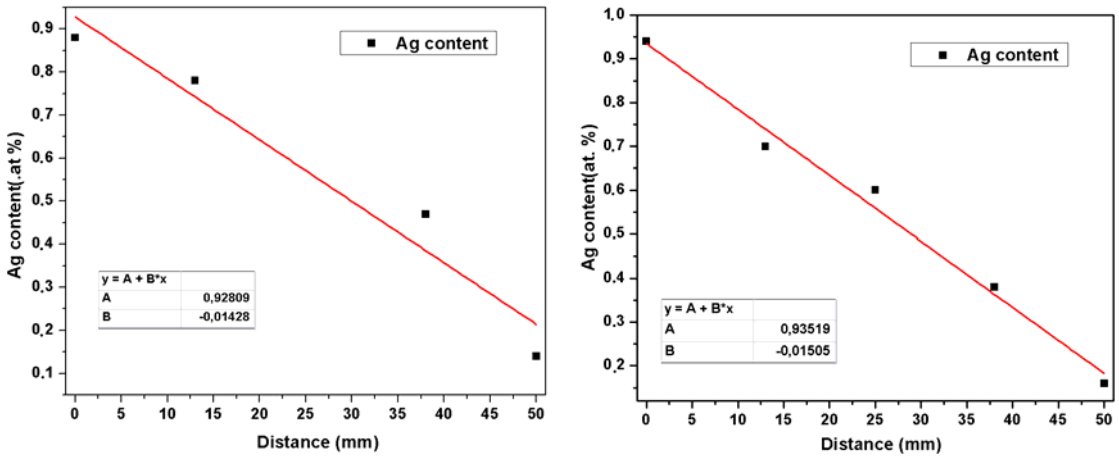

Fig. 6 Ag content profiles determined by EDS for film areas between A and B points of Ag-HA (left) and Ag-β-TCP (right) mm, c) 20 mm, d) 30mm, e) 40mm and f) 50 mm, respectively.

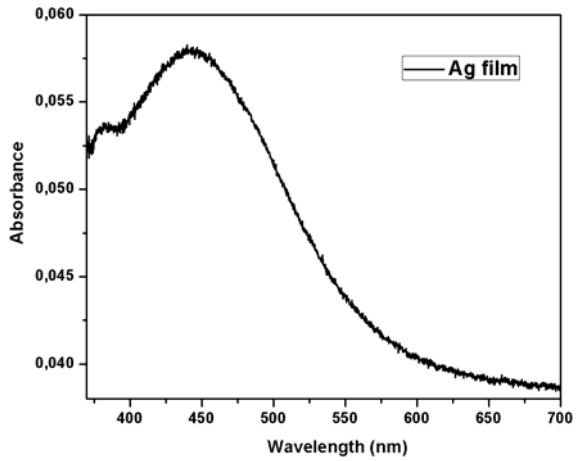

Fig. 7 Typical optical absorption spectrum of Ag film deposited on glass.

Multi-element X-ray mapping images acquired by EDS were used to identify the elemental distribution along the surface. We give in Figs. 8 and 9 selected areas from SEM micrographs and corresponding element mapping images at boundaries, "A" and "B" positions, where Ca, P and Ag in Ag-HA and Ag- β-TCP samples were clearly put into evidence. Several similarities and peculiarities characteristic to each sample are visible in Figs 8 and 9. Because at "A" position (Figs. 8-9 left columns), the size and density of particulates are smaller, the distribution of Ca, P and Ag elements looks rather homogenous over the investigated area. At "B" position (Figs. 8-9 right columns) the increase in size and density of CaP particulates stay at the origin of the elemental distribution variation along surface. Thus, the surface and the shape of the large particulates which are visible in the SEM micrographs are reflected by the element mapping images. Ca and P distribution in the elemental mapping images of Ag-HA samples recorded at "B" position (Fig. 8 right column) show an increased abundance in the areas where the particulates are located. We thus could conclude that the mass density of HA particulates is larger than that of the homogeneous part of the coating. Unlike Ag-HA samples, in the case of Ag- β-TCP films, the elemental mapping for Ca and P elements (Fig. 9 right column) showed that besides their different contour, the particulates have similar or slightly lower mass density than that of the homogeneous

film. The increase of the mass density at the particulates boundary is a result of densification by accumulation of material from the craters, due to deep penetration into film. The densification effect of craters' walls was more evident in the case of Ag- β-TCP samples because these coatings were softer and/or less dense than HA films. The fraction of particulates which are embedded into the coatings does not generate craters because they were transferred during the early stage of the film formation [39, 40]. Ag abundance (Figs.8-9) in the areas around “A” and “B” was uniformly distributed for both types of samples. Ag particulates were not visible in the elemental mapping images because their dimensions were under the pixel resolution.

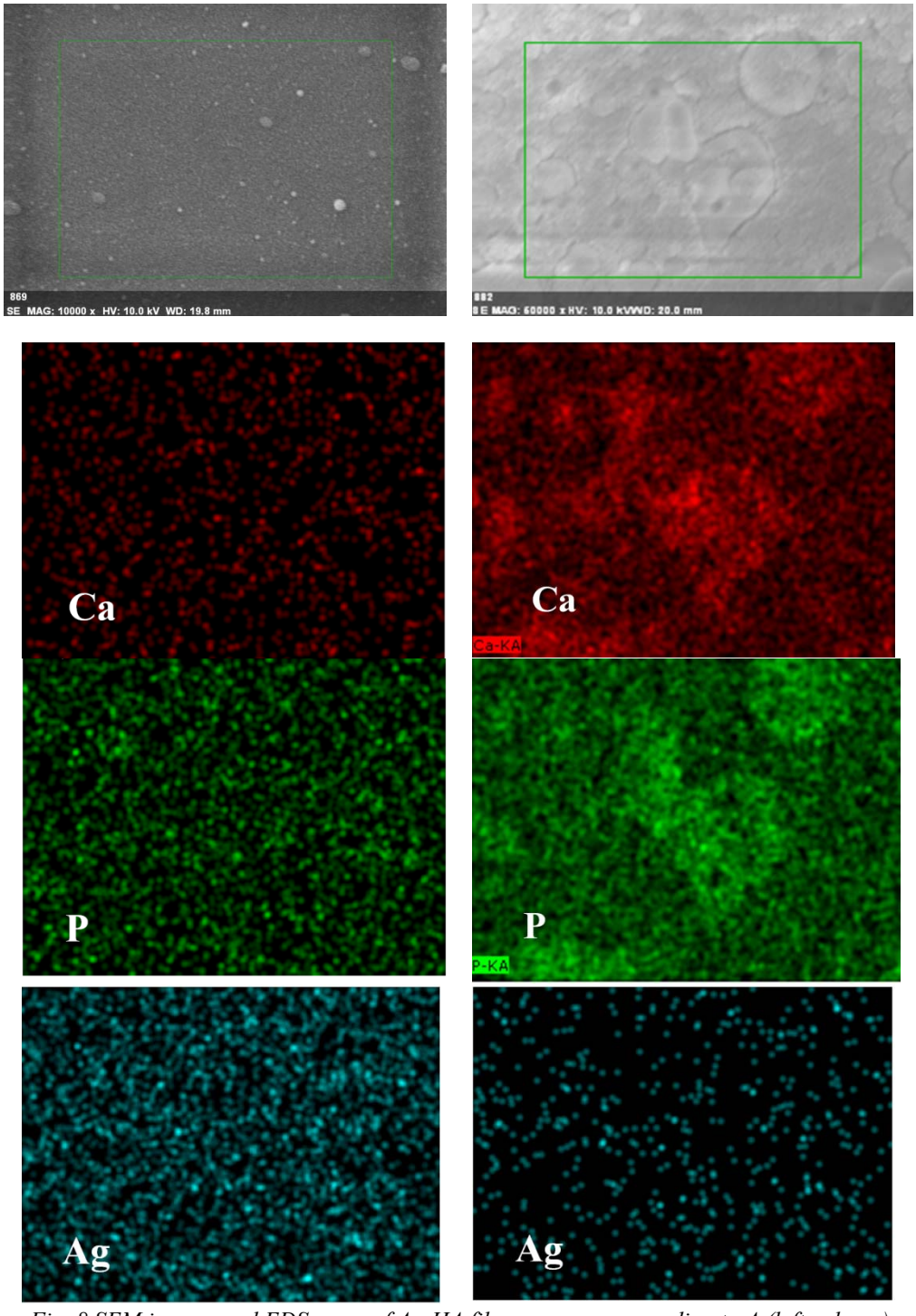

Fig. 8 SEM images and EDS maps of Ag-HA film areas corresponding to A (left column) and B (right column) positions.

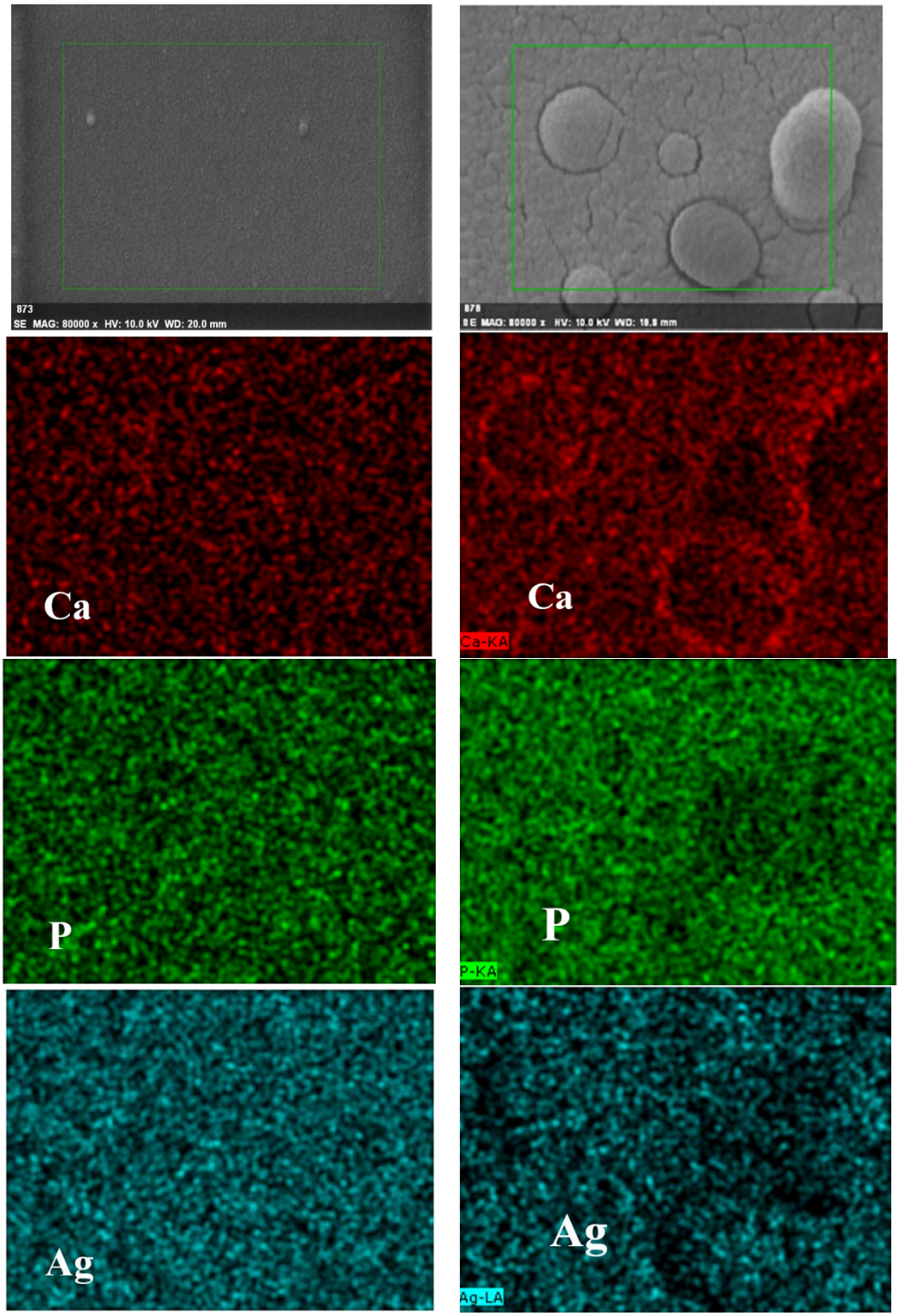

Fig. 9 SEM images and EDS maps of Ag-β-TCP film areas corresponding to A (left column) and B (right column) positions.

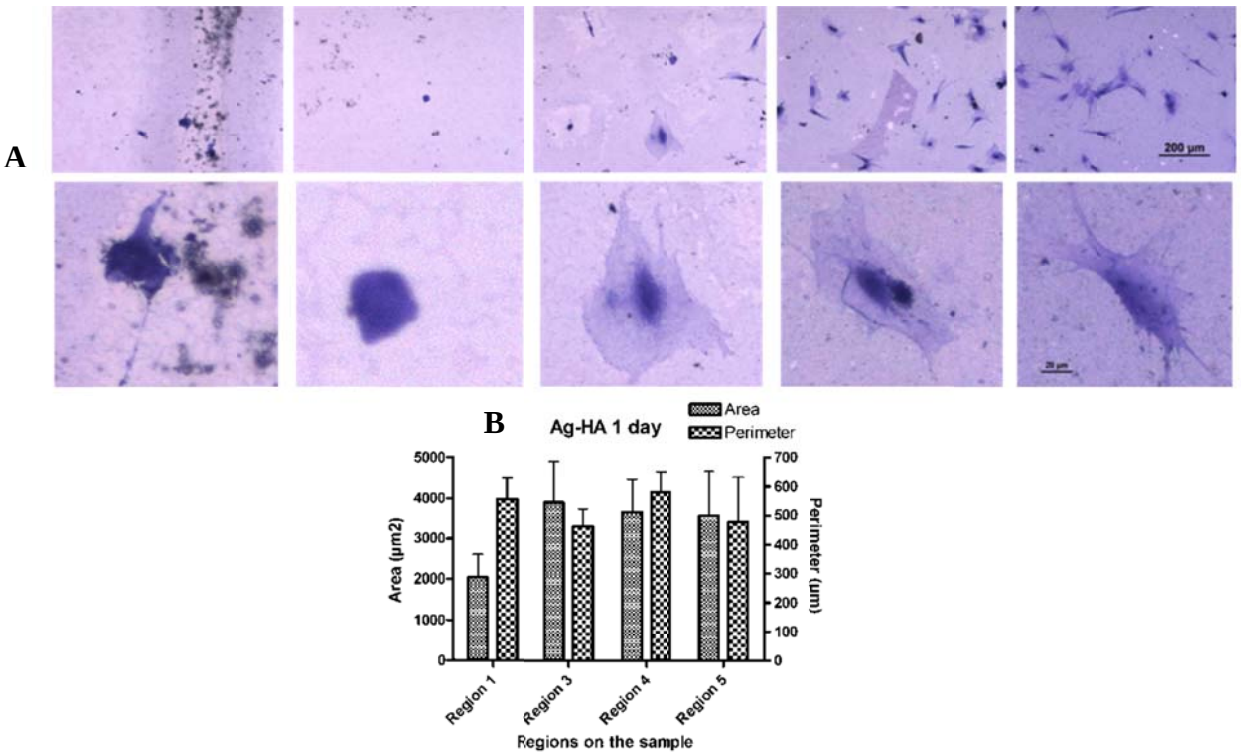

Fig.10 A -top and -bottom panels show the optical images of MSCs grown on Ag-HA recorded at a magnitude of 100 x and 500 x, respectively. B - Quantification of cell areas and perimeters for MSC visible in A at 24h after seeding.

Biological results

Biological studies were performed in order to test how human MSCs respond to biomaterial coatings. As known, while osteosarcoma and transformed osteoblasts are directly used in *in vitro* biocompatibility assays, MSCs come in close contact with the implant and give rise to bone-forming cells. Based upon a statistical analysis it was determined whether MSCs morphology (perimeter or area of cells) was altered by the variation of Ag content and surface morphological features along the "AB" direction of Ag-containing CaP coatings. Cells morphology on each sample was assessed by quantifying cells area and perimeter between "A" and "B" points. Thus, the surface of samples was divided in regions of equal areas starting from "A" (0 mm) to "B" (50 mm) positions. Five separated regions were considered: Region I (0 mm-10 mm), Region II (10 mm-20 mm), Region III (20 mm-30 mm), Region IV (30 mm-40 mm) and Region V (40 mm-50 mm), respectively (see Fig. 10). Due to known differences between the two CaP's solubility, the bone cells attachment was investigated after 3h, 6h and 24h of incubation for the more soluble Ag-β-TCP coatings or 24 h for more stable Ag-HA coatings. Representative images of bone cells grown on Ag-HA were collected by bright field microscopy and are shown in Fig. 10A – top panel. Details of cell morphology are magnified in Fig 10A – bottom panel. Also, statistics of cell areas and perimeters from different regions of combinatorial samples were represented as bar graphs (Fig.10B).

One observes that after 24 h, the cell attachment parameters at the contact with the surface of Ag-HA samples (Fig.10B) exhibit large values. The cells area varied within 2000-4000 μm^2 range whereas the cells perimeter was measured in a narrow interval between 480-600 µm. In the Region I, where the maximum Ag content was found, the ratio between area (2000 μm^2) and perimeter (580 µm) is the smallest of all analyzed regions. Such morphology is characteristic for elongated cells or with multiple cellular extensions. The cells behavior in Regions III-V was

similar but their area and perimeter values were typical for cellular morphologies with a more compact and regular shape. Moreover, the number of cells constantly increased from Region I to Region V (Fig.10A– top panel). At variance, in the case of Ag-β-TCP coatings we observed at 3h, 6h and 24 h partial cell attachment, but MSCs-coating interaction was not sufficiently stable to support cell growth and proliferation (data not shown). At the surface of β-TCP coatings a morphological and chemical instability develops due to the greater solubility which could stay at the origin of the poor cellular attachment. We consider that the reduced biological response of Ag-β-TCP samples after 6h and 24h of incubation is a consequence of the fast β-TCP dissolution in the surrounding cellular solution. From the above results one may conclude that Ag from the calcium phosphate coatings is not toxic for MSCs in concentrations up to ~ 0.6 at. % (Regions III-V). The topological features of CaP coatings deposited by PLD and their solubility properties (HA vs TCP) drastically influenced the cellular attachment and morphology.

4. Conclusions

The specific topology of CaP coatings deposited by PLD, consisting of grains with tens or hundreds of nanometers in size and combined with the presence of irregular particulates with dimensions in the sub- micronic and micronic ranges, proved beneficial for adhesion and proliferation of MSCs. We observed that the solubility of CaP coatings deposited at room temperature has a drastic influence on the adhesion and cellular morphology of MSCs. Thus, the more soluble β-TCP coating was not sufficiently chemically stable to support cell growth and proliferation. We demonstrated that Ag content of up to 0.6 at. % into HA coatings deposited by PLD could be considered nontoxic for MSCs.

Acknowledgments

Gabriel Socol gratefully acknowledges the European Social Fund POSDRU 2007-2013 through the contract POSDRU/89/1.5/S/60746. This work was partially supported by the grant of the Romanian National Authority for Scientific Research, CNCS-UEFISCDI, project number PN-II-ID-PCE-2011-3-0888 (209/5.10.2011). Felix Sima acknowledges the support of the contract PN-II-RU-PD-2011-3-0147 (101/2012).

References

[1] J-A.Epinette, M. T. Thomas, Fifteen years of clinical experience with hydroxyapatite coatings in joint arthroplasty, Springer Verlag, France (2004).
[2] B. Leon, A. J. Jansen (Ed.), Thin Calcium Phosphate Coatings for Medical Implants, Springer Science + Business Media, New York (2009).
[3] V. Nelea, M. Jelinek, I. N. Mihailescu, Chapter 9 (p. 265) in Pulsed laser deposition of optoelectronic films, Series: Optoelectronic Materials and Devices, 2 (2005).
[4] R. Eason (Ed.), Pulsed Laser Deposition of thin films: applications-led growth of functional materials, John Wiley & Sons, New Jersey (2007).
[5] S.V. Dorozhkin, J. Mater. Sci. **42,** 1061 (2007).
[6] S.V. Dorozhkin, Materials **2**, 1975 (2009).
[7] S.V. Dorozhkin., Materials **2**, 399 (2009).
[8] G. Daculsi, Biomaterials **19**, 1473 (1998).
[9] G. Daculsi, O. Laboux, O. Malard, P. Weiss, J. Mater. Sci. Mater. Med. **14**, 195 (2003);
[10] R.Z. LeGeros, S. Lin, R. Rohanizadeh, D Mijares, J.P. LeGeros, J. Mater. Sci. Mater. Med. **14**, 201 (2003).
[11] J. Dong, T. Uemura, Y. Shirasaki, T. Tateishi, Biomaterials **23,** 4493 (2002).
[12] Hassna R.R. Ramay, M. Zhang, Biomaterials **25**, 5171 (2004).
[13] DA LaVan, T McGuire, R. Langer, Nature Biotechnology **21**(10), 1184 (2003).
[14] R. Cristescu, C. Popescu, G. Socol, A. Visan, I.N. Mihailescu, S.D. Gittard, P.R. Miller, T.N. Martin, R.J. Narayan, A. Andronie, I. Stamatin, D.B. Chrisey, Applied Surface Science

257, 5287 (2011).
[15] R. Cristescu, C. Popescu, G. Socol, I. Iordache, I.N. Mihailescu, D.E. Mihaiescu, A.M. Grumezescu, A. Andronie, I. Stamatin, C. Chifiriuc, C. Bleotu, C. Saviuc, M. Popa, D.B. Chrisey, In press in Applied Surface Science.
[16] A. Mostafa, H. Oudadesse, Y. Legal, E. Foad, G. Cathelineau, Bioceramics Development and Applications 1 D101128 (2011).
[17] K. Krupa-Żuczek, K. Bialik-Wąs, A. S. Kupiec, M. Piątkowski, M. Zimowska, B. Tyliszczak, Digest Journal of Nanomaterials and Biostructures **6**(4) 1725 (2011).
[18] Kyu-Seog Hwang, Seung Hwangbo, Jin-Tae Kim, J Nanopart Res 101337 (2008).
[19] Y. Ando, H. Miyamoto, I. Noda, N. Sakurai, T. Akiyama, Y. Yonekura, T. Shimazaki, M. Miyazaki, M. Mawatari, T. Hotokebuchi, Materials Science and Engineering C **30**, 175 (2010)
[20] C. Greulich, J. Diendorf, J. Geßmann, T. Simon, T. Habijan, G. Eggeler, T.A. Schildhauer, M. Epple, M. Köller, Acta Biomaterialia **7**, 3505 (2011).
[21] A. Ewald, D. Hösel, S. Patel, L. M. Grover, J. E. Barralet, U. Gbureck, Acta Biomaterialia **7**, 4064 (2011).
[22] J.J. Blaker, S.N. Nazhat, A.R. Boccaccini, Biomaterials **25**,1319 (2003).
[23] J. Hardes, H. Ahrens, C. Gebert, A. Streitbuerger, H. Buerger, M. Erren, A. Gunseld, C. Wedemeyere, G. Saxlere, W. Winkelmanna, G. Gosheger, Biomaterials **28**, 2869 (2007).
[24] B. Jansen, M. Rinck, P. Wolbring, A. Strohmeier, T. Jahns, J Biomater App **l9,** 55 (1994).
[25] V. Stanica, D. Janackovicb, S. Dimitrijevicb, S.B. Tanaskovicc, M. Mitrica, M. S. Pavlovica, A. Krsticd, D. Jovanovice, S. Raicevi, Applied Surface Science **257,** 4510 (2011).
[26] E. Vernea, S. Di Nunzio, M. Bosetti, P. Appendino, C. Vitale Brovarone, G. Maina, M. Cannas, Biomaterials **26,** 5111 (2005).
[27] A. M. El-Kady, A. F. Ali, R. A. Rizk, M. M. Ahmed, Ceramics International **38**, 177 (2012).
[28] L. Baia, M. Baia, W. Kiefer, J. Popp, S. Simon, Chemical Physics **327**, 63(2006).
[29] V. Nelea, H. Pelletier, D. Muller, N. Broll, P. Mille, C. Ristoscu, I.N. Mihailescu, Applied Surface Science **186**(1-4), 483 (2001).
[30] A. Bigi, B. Bracci, F. Cuisinier, R. Elkaim, M. Fini, I. Mayer, I.N. Mihailescu, G. Socol, L. Sturba, P. Torricelli, Biomaterials **26**, 2381 (2005).
[31] I. N. Mihailescu, P. Torricelli, A. Bigi, I. Mayer, M. Iliescu, J. Werckmann, G. Socol, F. Miroiu, F. Cuisinier, R. Elkaim, G. Hildebrand, Applied Surface Science **248**, 344 (2005).
[32] F. Sima, G. Socol, E. Axente, I.N. Mihailescu, L. Zdrentu, S.M. Petrescu, I. Mayer, Applied Surface Science 254(4) 1155 (2007).
[33] G. Socol, A.C. Galca, C.R. Luculescu, A. Stanculescu, M. Socol, N. Stefan, E. Axente, L. Duta, C.M. Mihailescu, V. Craciun, D. Craciun, V. Sava, I.N. Mihailescu, Digest Journal of Nanomaterials and Biostructures **6**(1) 107 (2011).
[34] E. Gyorgy, P. Toricelli, G. Socol, M. Iliescu, I. Mayer, I. N. Mihailescu, A. Bigi, J. Werckman, Journal of Biomedical Materials Research Part A **71A**(2) 353 (2004).
[35] S. Wang, S. Boussaad, and N.J. Tao, Review of Scientific Instruments **72**(7) (2001)
[36] S.L. Smitha, K.M. Nissamudeen, D. Philip, K.G. Gopchandran, Spectrochimica Acta Part A **71,** 186 (2008).
[37] W.A. Weimer, M.J. Dyer, Appl. Phys. Lett. **79**, 3164 (2001).
[38] M. Brown, M. Shiloh, R.B. Jackman, I.W. Boyd, Applied Surface Science **43**, 382 (1989).
[39] I.N. Mihailescu, P. Torricelli, A. Bigi, I. Mayer, M. Iliescu, J. Werckmann, G. Socol, F. Miroiu, F. Cuisinier, R. Elkaim, G. Hildebrand, Applied Surface Science **248,** 344 (2005).
[40] M. Iliescu, V. Nelea, J. Werckmann, IN. Mihailescu, G. Socol, A. Bigi, B. Bracci, Thin Solid Films 453157 (2004).